I.J. Wireless and Microwave Technologies, 2025, 6, 27-40
Published Online on December 8, 2025 by MECS Press (http://www.mecs-press.org/)
DOI: 10.5815/ijwmt.2025.06.03

Empowering Next-Gen Networks: Unleashing the Potential of SWIPT-Enabled Energy Harvesting in Collaborative Cognitive Radio-NOMA Networks

Huu Q. Tran*
Faculty of Electronics Technology, Industrial University of Ho Chi Minh City, Vietnam
E-mail: tranquyhuu@iuh.edu.vn;
ORCID iD: https://orcid.org/0000-0001-7636-4378
*Corresponding Author

Lam Hoang Kham
Faculty of Electronics Technology, Industrial University of Ho Chi Minh City, Vietnam
E-mail: hoangkhamlam0509@gmail.com

Received: 01 November, 2024; Revised: 13 April, 2025; Accepted: 01 August, 2025; Published: 08 December, 2025

Abstract: The convergence of Non-Orthogonal Multiple Access (NOMA) and Cognitive Radio (CR) with Simultaneous Wireless Information and Power Transfer (SWIPT) offers a transformative approach to spectrum and energy efficiency. This paper analyzes CR–NOMA with SWIPT-enabled energy harvesting (EH), focusing on outage probability (OP) and throughput. We derive explicit models under Rayleigh fading with interference-temperature constraints and validate by simulations. Results show that proper power allocation and time-switching ratios enhance user fairness while respecting primary-network interference. These insights guide robust and energyefficient designs for next-generation systems.

Index Terms: Cognitive Radio (CR), Collaborative Relaying, Energy Harvesting (EH), Message Processing (MP) Non-Orthogonal Multiple Access (NOMA), Simultaneous Wireless Information and Power Transfer (SWIPT)

1. Introduction

Non-Orthogonal Multiple Access (NOMA) has emerged as a compelling multiple-access paradigm for next-generation wireless systems due to its ability to multiplex users in the power domain and hence improve spectral efficiency and user fairness compared with orthogonal schemes [1–3]. Unlike conventional OMA (e.g., FDMA/TDMA), NOMA allows multiple devices to share the same time–frequency resources simultaneously while the receiver employs successive interference cancellation (SIC) to separate superposed signals. In practical deployments, this enables serving near and far users concurrently, improving aggregate throughput while guaranteeing a minimum service level for cell-edge users. These properties make NOMA a strong candidate for 5G-and-beyond heterogeneous networks supporting massive connectivity and diverse QoS requirements [4–7].

Simultaneous Wireless Information and Power Transfer (SWIPT) provide a complementary dimension to spectrum efficiency by enabling radio-frequency (RF) signals to carry both information and usable energy [8–11]. In SWIPT receivers, part of the received signal is converted to DC power to charge energy-limited devices (e.g., IoT nodes), while the rest is used for data decoding. This dual use of RF resources eliminates frequent battery replacement and significantly enhances network sustainability. However, coordinating the split between energy harvesting (EH) and information decoding introduces new design trade-offs, motivating extensive studies on SWIPT-enabled cooperative and NOMA systems [12–15].

Cooperative relaying (RC) enhances link coverage and reliability by allowing intermediate nodes to assist end-to-end transmission [16–18]. When combined with SWIPT, relays become self-sustainable by harvesting energy from received signals, reducing external power demand and improving deployment feasibility in harsh environments. Such SWIPT–RC–NOMA architectures, when optimized, unlock substantial gains in throughput, outage performance, and energy efficiency [19–21].

1.1 Related work and open issues.

A number of studies have explored different facets of SWIPT-enabled NOMA and cooperative relaying. For example, downlink outage characterization with EH at the near user is provided in [22], while [23] studies PS-based throughput and EH optimization for IIoT devices. Wireless energy-harvesting (WEH) relaying performance was analyzed in [24], whereas socially aware MEC-assisted NOMA-EH was addressed in [25]. Energy-efficient resource allocation for SWIPT-enabled massive MIMO systems was discussed in [26].

In cognitive radio (CR) systems, diversity combining, DF/AF relay selection, and relay-sharing schemes under interference constraints have been reported in [27–29]. Bidirectional AF relaying with underlay sharing has been characterized in [30], while secrecy-enhanced hybrid-EH designs appear in [31] and [32]. Collaborative wireless-powered NOMA schemes have also shown significant outage gains [33]. OFDM-based relaying, SWIPT-driven OFDMA resource allocation, and related multi-hop enhancements are additionally discussed in [34] and [35]. Classical mathematical tools frequently used for deriving tractable expressions (e.g., special integrals, gamma functions) follow from [36].

Despite these advances, several gaps remain for collaborative cognitive SWIPT–NOMA systems with explicit energy–information time structuring at the relay:

(i) The joint interaction among interference-temperature constraints, NOMA power allocation, and EH scheduling produces complex feasibility regions that are not yet fully characterized analytically;

(ii) Time-switching relaying (TSR), although hardware-efficient, lacks comprehensive outage/throughput/ergodic-rate analyses under CR underlay constraints;

(iii) Unified analytical insights capturing OP, system throughput (ST), ergodic rate (ER), and energy efficiency (EE) under a common channel–interference framework are still limited.

1.2 Contributions

Motivated by the above, this paper develops a tractable analytical framework for a collaborative CR–NOMA network with SWIPT-enabled half-duplex relaying operating under an underlay interference constraint. We adopt the TSR protocol at the relay to decouple EH and message processing in time, and we incorporate NOMA superposition coding with SIC at the forwarding stage. The main contributions are:

- We formulate an underlay CR–NOMA system where the secondary source (S) superposes messages for two destinations (D1, D2) and a relay (R) harvests energy during an αT sub-block (TSR) before forwarding. The interference-temperature constraint at the primary destination (PD) limits the instantaneous secondary transmit power, capturing a realistic PU-protection mechanism.
- We derive explicit closed-form or series-form expressions for the outage probability of both destinations, carefully accounting for the SIC feasibility condition, the TSR-induced harvested-power level at R, and the underlay constraint on S. The results quantify how EH time fraction, NOMA power allocation, and interference budget jointly shape reliability.
- Building on the OP analysis, we provide expressions for delay-limited throughput (ST) and delay-tolerant ergodic rate (ER) for both users. We further define and evaluate a consistent energy efficiency (EE) metric that relates the aggregate achievable rate to the total consumed/harvested power across S and R.
- Through Monte Carlo simulations, we validate the analytical expressions and reveal operating regimes where the TSR fraction and NOMA allocation coefficients yield favorable reliability–throughput–efficiency trade-offs, offering concrete design guidelines for CR–NOMA systems with EH relays.

1.3 System assumptions and scope

Unless otherwise stated, all links experience Rayleigh fading and nodes operate with single antennas; perfect CSI and perfect SIC are assumed following standard baselines [1–3]. The CR underlay constraint is modeled using an instantaneous interference-temperature ceiling. TSR-based EH is adopted for analytical tractability, while nonlinear EH behaviors follow insights from [32–34].

1.4 Organization

Section 2 presents the system model. Section 3 provides OP, ST, ER, and EE analyses. Section 4 discusses simulation results. Section 5 concludes the paper. Proofs appear in the Appendices.

2. System Model

Figure 1 illustrates the system model under examination. This model comprises a PD located within the primary network (PN), a secondary source (S), a relay node (R) operating in half-duplex mode, and two destinations, D_1 and D_2. We denote c_{SD}, c_{SR}, c_{RD1}, c_{RD2} as the complex channel coefficients representing the channels S → PD, S → R, R → D_1, and R → D_2, respectively. Throughout, $\{c_{XY}\}$ are modeled as zero-mean i.i.d. circularly symmetric complex Gaussian RVs with variances Ωc_{XY} = E[$|c_{XY}|^2$] (i.e., Rayleigh power gains), unless stated otherwise. Assuming each node uses only one antenna, perfect channel state information (CSI) is available at receivers. It is also assumed that R is placed far from the PD, and thus it cannot interfere with the primary network as shown in Figure 1. Both the primary and secondary networks are subject to transmit-power and interference-temperature constraints. The notation used in this section follows Table 1.

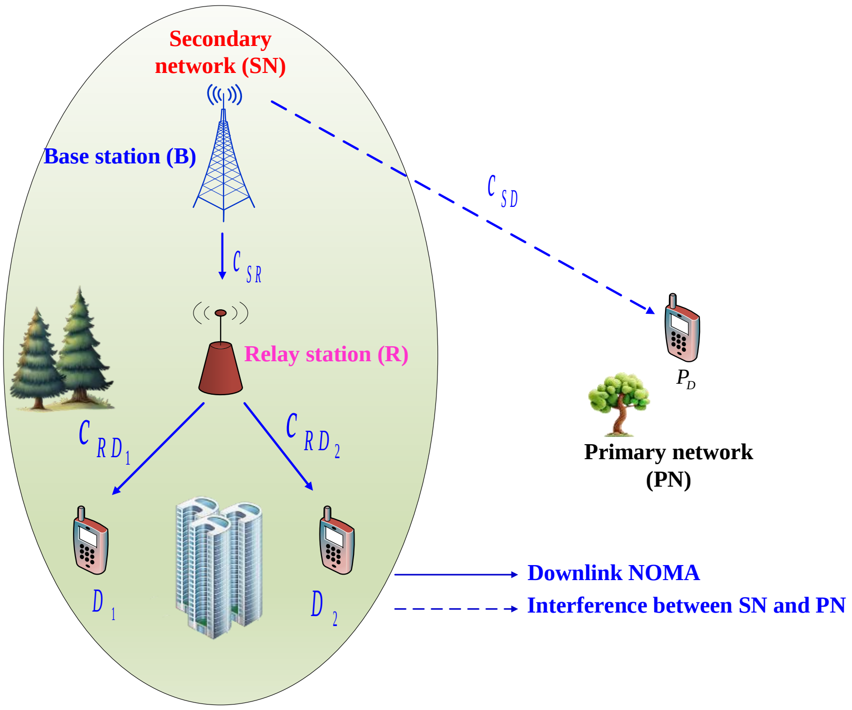

Fig. 1. System model.

In this context, the expectation operation, denoted as E[.], signifies the average or mean value of the specified quantity. According to the NOMA principle in the first phase, S transmits a superposition-coded signal for D_1 and D_2:

$$X_S(t)=\sqrt{P_S\alpha_1}x_1(t)+\sqrt{P_S\alpha_2}x_2(t), \tag{1}$$

with the instantaneous power constrained by the primary link:

$$P_S \le \min\left(\frac{I}{|c_{SD}|^2},\overline{P_S}\right), \tag{2}$$

where $\overline{P_S}$ is the maximum average transmit power at S, and I is the maximum allowable interference temperature at PD. Here, α_1 and α_2 are the NOMA power-allocation coefficients for D_1 and D_2 with $\alpha_1 + \alpha_2 = 1$ and $\alpha_1 > \alpha_2$; x_1 and x_2 are unit-power symbols. The received signal at R (first time slot) is

$$Y_R(t)=c_{SR}X_S(t)+w_R^{[r]}(t)=c_{SR}\left[\sqrt{P_S\alpha_1}x_1(t)+\sqrt{P_S\alpha_2}x_2(t)\right]+w_R^{[r]}(t) \tag{3}$$

where $w_R^{[r]}(t)$ is AWGN at R with variance σ^2. We define $\rho_s \triangleq \frac{P_s}{\sigma^2}$ as the transmit SNR.

2.1 *EH at R*

At R, we evaluate SWIPT using the time-switching relaying (TSR) protocol.

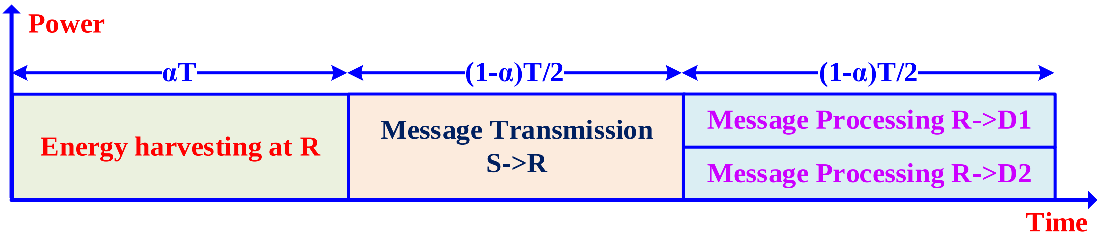

Fig. 2. The TSR protocol for energy harvesting (EH) and message processing (MP) at the relay.

Figure 2 illustrates the key timing parameters. The harvested energy at R is

$$E_h = \eta \overline{P}_S \left|c_{SR}\right|^2 \alpha T, \tag{4}$$

and the relay transmit power in the forwarding phase is

$$P_R = \frac{E_H}{(1-\alpha)T/2} = \frac{\eta \overline{P}_S \left|c_{SR}\right|^2 \alpha T}{(1-\alpha)T/2} = \frac{2\eta \overline{P}_S \left|c_{SR}\right|^2 \alpha}{(1-\alpha)}, \tag{5}$$

where T is the block duration and $\eta \in (0,1]$ is the RF-to-DC conversion efficiency. In the TSR protocol, the first sub-block αT is for EH and S→*R* reception; the remaining duration $(1-\alpha)T$ is used for relaying, equally split into R→D_i transmission and destination processing intervals. For convenience, define the EH gain factor $\psi_E = \frac{2\eta\alpha}{(1-\alpha)}$.

2.2 *MP at R*

The baseband sample at R including RF and circuit noise is

$$\begin{aligned} Y_{IP,R}(k) &= c_{SR} X_S(k) + w_R^{[r]}(k) + w_C^{[r]}(k) \\ &= c_{SR}\left[\sqrt{P_S\alpha_1}x_1(k) + \sqrt{P_S\alpha_2}x_2(k)\right] + w_R^{[r]}(k) + w_C^{[r]}(k), \end{aligned} \tag{6}$$

where $w_C^{[r]}(k)$ accounts for additional receiver circuitry noise. Following the NOMA principle, D_1 is allocated more power than D_2. R first decodes x_1 treating x_2 as interference, then applies SIC to decode x_2:

$$\gamma_{R,x_1} = \frac{\rho_S \alpha_1 \left|c_{SR}\right|^2}{\rho_S \alpha_2 \left|c_{SR}\right|^2 + 1}, \gamma_{R,x_2} = \rho_S \alpha_2 \left|c_{SR}\right|^2 \tag{7}$$

2.3 *MP at D1 and D2*

In the second slot, R forwards the detected symbols to D_1 and D_2 with superposition:

$$\begin{aligned} Y_{D_i}(k) &= c_{RD_i} X_R(k) + w_R^{[d]}(k) + w_C^{[d]}(k) \\ &= c_{RD_i}\left|c_{SR}\right|\sqrt{\psi_E \overline{P_S}}\left(\sqrt{\alpha_1}x_1(k) + \sqrt{\alpha_2}x_2(k)\right) + w_R^{[d]}(k) + w_C^{[d]}(k), \end{aligned} \tag{8}$$

where ($w_R^{[d]}(k), w_C^{[d]}(k)$) are AWGN and circuit noise at destinations. Let $\overline{\rho_S} = \frac{\overline{P_S}}{\sigma^2}$ denote the effective SNR scale on the R→D_i hop under EH. Then the destination-side SINRs are

$$\gamma_{RD_1,x_1} = \frac{\overline{\rho_S}\alpha_1 \left|c_{SR}\right|^2 \left|c_{RD_1}\right|^2 \psi_E}{\overline{\rho_S}\alpha_2 \left|c_{SR}\right|^2 \left|c_{RD_1}\right|^2 \psi_E + 1}, \gamma_{RD_2,x_1} = \frac{\overline{\rho_S}\alpha_1 \left|c_{SR}\right|^2 \left|c_{RD_2}\right|^2 \psi_E}{\overline{\rho_S}\alpha_2 \left|c_{SR}\right|^2 \left|c_{RD_2}\right|^2 \psi_E + 1}, \tag{9}$$

and

$$\gamma_{RD_2,x_2} = \overline{\rho_S}\alpha_2 |c_{SR}|^2 |c_{RD}|^2 \psi_E, \tag{10}$$

3. Performance analysis of the TSR protocol

3.1 Outage Performance

3.1.1 OP at D_1

In NOMA, D_1 avoids outage if both x_1 (at R) and the forwarded x_1 (at D_1) are decoded successfully. Hence,

$$OP_{D1} = \Pr[\min(\gamma_{R,x_1}, \gamma_{RD_1,x_1}) < \gamma_1] = 1 - \Pr(\gamma_{R,x_1} > \gamma_1, \gamma_{RD_1,x_1} > \gamma_1), \tag{11}$$

where $\gamma_1 = 2^{R_1} - 1$ corresponds to the target rate D_1 for x_1.

Theorem 1 *The OP at D_1 admits the following representation:*

$$OP_{D_1} = 1 - \left[\begin{array}{l} \left[\left(1 - e^{-\frac{\rho_I}{\overline{\rho_S}\Omega_{C_{SD}}}}\right) \sum_{n=0}^{\infty} \frac{(-1)^n}{\left(\Omega_{C_{SR}}\right)^{n+1} n!} \mu_1^{n+1} \gamma\left(-n-1, \frac{\mu_1 \psi}{\overline{\rho_S}}\right)\right] \\ + \left[\sum_{n=0}^{\infty} \frac{(-1)^n}{\left(\Omega_{C_{SR}}\right)^{n+1} n!} \mu_1^{n+1} \int_{\frac{\rho_I}{\rho_S}}^{\infty} \frac{1}{\Omega_{C_{SD}}} e^{-\frac{x}{\Omega_{C_{SD}}}} \gamma\left(-n-1, \frac{\mu_1 \rho_I}{\psi x}\right) dx\right] \end{array}\right], \tag{12}$$

where $\psi = \frac{\gamma_1}{\alpha_1 - \gamma_1 \alpha_2}$ $(Vaild\ for \alpha_1 > \gamma_1 \alpha_2)$, $\mu_1 = \frac{\psi}{\psi_E \rho_S \Omega_{C_{RD_1}}}$, $and\ \rho_I \triangleq I/\sigma^2$

Proof See Appendix A.

3.1.2 OP at D2

D_2 succeeds only if both R and D_2 can decode x_2:

$$OP_{D_2} = \Pr[\min(\gamma_{R,x_2}, \gamma_{RD_2,x_2}) < \gamma_2] = 1 - \Pr(\gamma_{R,x_2} > \gamma_2, \gamma_{RD_2,x_2} > \gamma_2), \tag{13}$$

where $\gamma_2 = 2^{R_2} - 1$ is set by the target rate D_2 for x_2.

Theorem 2 The OP at D_2 can be written as

$$OP_{D_2} = 1 - \left[\begin{array}{l} \left[\left(1 - e^{-\frac{\rho_I}{\overline{\rho_S}\Omega_{C_{SD}}}}\right) \sum_{n=0}^{\infty} \frac{(-1)^n}{\left(\Omega_{C_{SR}}\right)^{n+1} n!} \mu_2^{n+1} \gamma\left(-n-1, \frac{\mu_2 \psi}{\overline{\rho_S}}\right)\right] \\ + \left[\sum_{n=0}^{\infty} \frac{(-1)^n}{\left(\Omega_{C_{SR}}\right)^{n+1} n!} \mu_2^{n+1} \int_{\frac{\rho_I}{\rho_S}}^{\infty} \frac{1}{\Omega_{C_{SD}}} e^{-\frac{x}{\Omega_{C_{SD}}}} \gamma\left(-n-1, \frac{\mu_2 \rho_I}{\psi x}\right) dx\right] \end{array}\right], \tag{14}$$

where $\psi_1 = \frac{\gamma_2}{\alpha_2}$ *and* $\mu_2 = \frac{\psi_1}{\psi_E \overline{\rho_S} \Omega_{C_{RD_2}}}$.

Proof See Appendix B.

3.2 ST for Delay-Limited Transmission

In this mode, S transmits at fixed rates (D_1, D_2); the system throughput is

$$\tau = \left(1 - OP_{D_1}\right) D_1 + \left(1 - OP_{D_2}\right) D_2, \tag{15}$$

where OP_{D_1} and OP_{D_2} are given by (3.2) and (3.4).

3.3 ER for Delay-Tolerant Transmission

3.3.1 ER at D1

If D_1 can decode x_2 at R (for SIC), its ergodic rate is

$$R_{D_1} = E\left[\log_2\left(1+\min\left(\gamma_{R,x_1},\gamma_{RD_1,x_1}\right)\right)\right] = \frac{1}{\ln 2}\int_0^\infty \frac{1-F_X(x)}{1+x}dx, \tag{16}$$

where $X \triangleq \min \gamma_{R,x_1}, \gamma_{R\,D_1,x_1}$ and F_x is its CDF. A computable form is:

$$R_{D_1} = \frac{1}{\ln 2}\left[\begin{array}{l}\left(1-e^{-\frac{\rho_I}{\rho_S \Omega_{c_{SD}}}}\right)\int_0^{\frac{\alpha_1}{\alpha_2}} \frac{1}{1+x}dx \int_{\frac{\tau}{\rho_S}}^{\infty} \frac{1}{\Omega_{c_{SR}}} e^{-\frac{y}{\Omega_{c_{SR}}}} e^{-\frac{\tau}{\psi_E \rho_S \Omega_{c_{RD_1}} y}} dy \\ +\int_0^{\frac{\alpha_1}{\alpha_2}} \frac{1}{1+x}dx \int_{\frac{\rho_I}{\rho_S}}^{\infty} \frac{1}{\Omega_{c_{SD}}} e^{-\frac{y}{\Omega_{c_{SD}}}} dy \int_{\frac{\tau y}{\rho_I}}^{\infty} \frac{1}{\Omega_{c_{SR}}} e^{-\frac{z}{\Omega_{c_{SR}}}} e^{-\frac{\tau}{\Omega_{c_{RD_1}} \rho_S \psi_E z}} dz\end{array}\right], \tag{17}$$

with $\tau \triangleq \psi = \frac{\gamma_1}{\alpha_1 - \gamma_1 \alpha_2}$

Proof See Appendix C.

3.3.2 ER at D2

Similarly,

$$R_{D_2} = E\left[\log_2\left(1+\min\left(\gamma_{R,x_2},\gamma_{RD_2,x_2}\right)\right)\right], \tag{18}$$

and one computable representation is

$$R_{D_2} = \frac{1}{\ln 2}\left[\begin{array}{l}\left(1-e^{-\frac{\rho_I}{\rho_S \Omega_{c_{SD}}}}\right)\int_0^{\frac{\alpha_1}{\alpha_2}} \frac{1}{1+x}dx \int_{\frac{\tau}{\rho_S}}^{\infty} \frac{1}{\Omega_{c_{SR}}} e^{-\frac{y}{\Omega_{c_{SR}}}} e^{-\frac{\tau_1}{\psi_E \rho_S \Omega_{c_{RD_2}} y}} dy \\ +\int_0^{\frac{\alpha_1}{\alpha_2}} \frac{1}{1+x}dx \int_{\frac{\rho_I}{\rho_S}}^{\infty} \frac{1}{\Omega_{c_{SD}}} e^{-\frac{y}{\Omega_{c_{SD}}}} dy \int_{\frac{\tau_1 y}{\rho_I}}^{\infty} \frac{1}{\Omega_{c_{SR}}} e^{-\frac{z}{\Omega_{c_{SR}}}} e^{-\frac{\tau_1}{\Omega_{c_{RD_2}} \rho_S \psi_E z}} dz\end{array}\right], \tag{19}$$

with $\tau_1 \triangleq \psi_1 = \frac{\gamma_2}{\alpha_2}$

Proof See Appendix D.

3.4 Energy Efficiency

We assess energy efficiency (EE) as the ratio of total achievable rate to the total consumed power:

$$EE \triangleq = \frac{R_{sun}}{P_S + P_R} \tag{20}$$

where $R_{sum} \in \left\{R_{D_1} + R_{D_2}\right\}$ for delay-limited / delay-tolerant modes.

With TSR-based EH, P_R is given by (2.5), and the dependence on α enters through $\psi_E = \frac{2\eta\alpha}{1-\alpha}$, enabling standard trade-off studies between harvesting time, outage/throughput, and EE.

4. Simulation Results

All Monte Carlo simulations are performed in MATLAB with 10^5 independent channel realizations per SNR point unless otherwise stated. Rayleigh fading is assumed for all links with mean power gains Ωc_{SR} , Ωc_{SD}, Ωc_{RD1} , and Ωc_{RD2}, and noise variance σ^2 =1 for normalization. The transmit SNR is defined as $\overline{\rho_S} = \frac{\overline{P_S}}{\sigma^2}$, the interference temperature at the primary destination is ρ_I, and the EH efficiency is η. The TSR factor is denoted by α. This section validates the derived expressions by comparing analysis with simulation. The simulation parameters were set with power allocation coefficients α_1 =0.82, α_2 =0.18, target rates R_1 =1 bps, R_2 =2 bps, and mean channel gain values (Ωc_{SR} , Ωc_{SD}, Ωc_{RD1} , Ωc_{RD2}) = (1,1,0.8,1). Unless specified, we take η = 0.8, α = 0.2, and an underlay interference cap ρ_I consistent with the primary protection constraint.

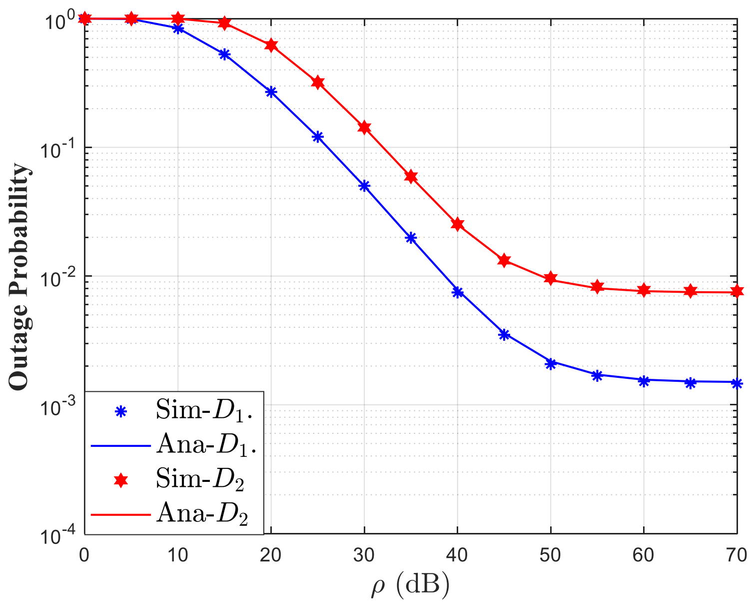

Fig. 3. OP versus transmit SNR ρS for D_1 and D_2.

Figure 3 shows that the outage probability (OP) at both D_1 and D_2 decreases rapidly as ρ_S increases and then exhibits an error floor at high SNR due to the underlay constraint ρ_I and the TSR-induced power coupling. The error floor level depends on ρ_I, α, and η. The analytical curves from (12) and (14) closely match the simulation markers across the entire SNR range, with a maximum gap below 0.5 dB. We also observe that stricter primary protection (smaller ρ_I) raises the OP floor, while larger α (more time for EH) can reduce the floor by boosting P_R via (5).

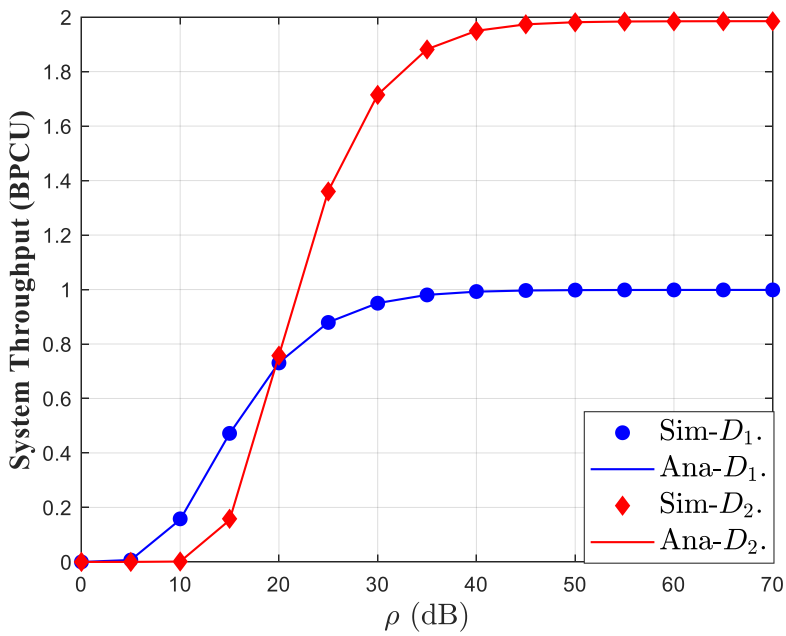

Fig. 4. System throughput versus transmitting SNR.

Figure 4 demonstrates the relationship between system throughput and SNR. D_2's throughput is initially lower than that of D_1 at low SNR; however, as ρ_S increases, D_2's throughput rises sharply and often approaches twice that of D_1 when α_2 is sufficiently large and SIC at R is reliable. This follows directly from the OP trends in (12)–(14) and the throughput definition in (15). Sensitivity tests (not shown) indicate that enlarging α or η improves τ at medium/high SNR by enhancing the relayed power P_R in (5), while too large α reduces the effective data phase $(1-\alpha)T$; thus, an optimal α exists.

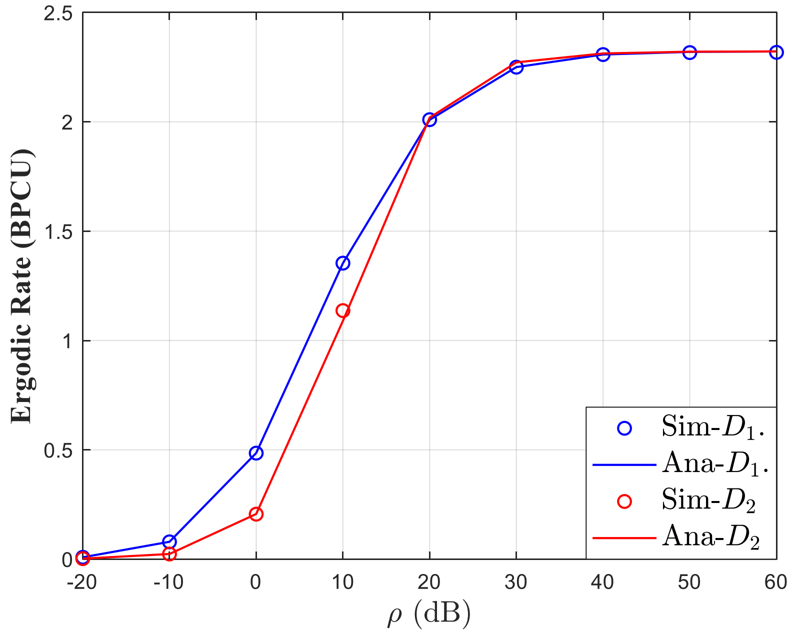

Fig. 5. Ergodic rate versus transmit SNR ρ_S.

Similar to Figure 4, Figure 5 illustrates the ergodic rate (ER) versus SNR. D_2 is initially inferior to D_1 in the low-SNR regime but catches up as ρ_S grows, approaching the D_1 ER around moderate/high SNR intervals when α_2 and ψ_E suffice to stabilize the relayed link. The trends are consistent with (17) and (19). We also verified that small residual-SIC penalties (not modeled here) primarily shift the curves rightward with negligible slope change.

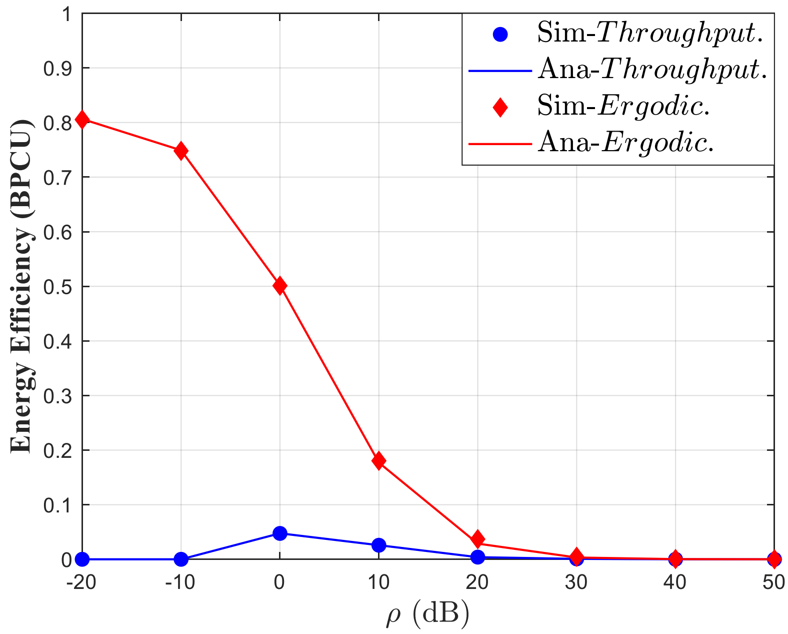

Fig. 6. Energy efficiency (EE) versus transmit SNR ρ_S.

Figure 6 compares the EE computed using ER- and ST-based rates. The system's EE in terms of both the ER and ST decreases rapidly as the SNR increases. The EE in terms of ER is higher than that in terms of ST, becoming equal and reaching the minimum value when ρ_S >30 dB. This is because the denominator grows with $P_S + P_R$ while the numerator saturates due to the underlay and time-sharing limits; see (20). In particular, PR scales with ψ_E via (5), which improves rate but also increases consumed power, yielding a non-monotonic EE–α trade-off. Overall, there exists an SNR window where TSR-based EH maximizes EE before the interference and harvesting overheads dominate.

5. Conclusion

This paper presented a tractable performance analysis of SWIPT-enabled CR–NOMA with TSR-based EH over Rayleigh fading. We derived exact and approximate expressions for the OP of D_1 and D_2 under an underlay interference constraint, and evaluated ST, ER, and EE across different SNR levels. Analysis and simulations showed close agreement, confirming the correctness of the derived formulas. Key insights include (i) OP floors at high SNR driven by ρ_I and time-sharing, (ii) a pronounced throughput/ER gain for the weak user D_2 at moderate-to-high SNR when α_2 and ψ_E are sufficiently large, and (iii) an EE optimum versus SNR and TSR factor α. Future work will incorporate nonlinear EH models, residual SIC, and robust designs under imperfect CSI, as well as multi-relay selection and IRS-assisted links.

Appendices

Notation used in Appendices. All links undergo Rayleigh fading with mean power gains $\Omega_{C_{XY}} \triangleq = E[|C_{XY}|^2]$. We define $\psi \triangleq \frac{\gamma_1}{\alpha_1-\gamma_1\alpha_2} (Vaild\ for\ \alpha_1 > \gamma_1\alpha_2\ )$, $\psi_1 \triangleq \frac{\gamma_2}{\alpha_2}, \mu_1 \triangleq \frac{\gamma_2}{\psi_E \rho_S \Omega_{C_{RD_1}}}, \mu_2 \triangleq \frac{\psi_1}{\psi_E \rho_S \Omega_{C_{RD_2}}}$, and use the lower incomplete gamma function γ(s,x) in the standard sense. The unit step is $U(x)$ = 1 for x > 0 and 0 for x < 0.

5.1 Appendix A – Proofs of Theorem 1 and Theorem 5

We have

$$OP_{D1} = \Pr[\min(\gamma_{R,x_1}, \gamma_{RD_1,x_1}) < \gamma_1] = 1 - P_r(\gamma_{R,x_1} > \gamma_1, \gamma_{RD_1,x_1} > \gamma_1)$$
$$= 1 - \left[\begin{array}{l} \Pr\left(\dfrac{\overline{\rho_S}\alpha_1 |c_{SR}|^2}{\overline{\rho_S}\alpha_2 |c_{SR}|^2 + 1} > \gamma_1, \dfrac{\overline{\rho_S}\alpha_1 |c_{SR}|^2 |c_{RD_1}|^2 \psi_E}{\overline{\rho_S}\alpha_2 |c_{SR}|^2 |c_{RD_1}|^2 \psi_E + 1} > \gamma_1, \overline{\rho_S} < \dfrac{\rho_I}{|c_{SD}|^2} \right) \\ + \Pr\left(\dfrac{\rho_I \alpha_1 |c_{SR}|^2}{\rho_I \alpha_2 |c_{SR}|^2 + |c_{SD}|^2} > \gamma_1, \dfrac{\overline{\rho_S}\alpha_1 |c_{SR}|^2 |c_{RD_1}|^2 \psi_E}{\overline{\rho_S}\alpha_2 |c_{SR}|^2 |c_{RD_1}|^2 \psi_E + 1} > \gamma_1, \overline{\rho_S} > \dfrac{\rho_I}{|c_{SD}|^2} \right) \end{array} \right] \tag{21}$$

Let

$$A_1 = P_r(|c_{SR}|^2 > \frac{\psi}{\overline{\rho_S}}, |c_{RD_1}|^2 > \frac{\psi}{\psi_E \overline{\rho_S} |c_{SR}|^2}, |c_{SD}|^2 < \frac{\rho_I}{\overline{\rho_S}})$$
$$= \int_{\frac{\psi}{\overline{\rho_S}}}^{\infty} f_{|c_{SR}|^2}(x)dx \int_{\frac{\psi}{\psi_E \overline{\rho_S} x}}^{\infty} f_{|c_{RD_1}|^2}(y)dy \int_0^{\frac{\rho_I}{\overline{\rho_S}}} f_{|c_{SD}|^2}(z)dz$$
$$= \int_{\frac{\psi}{\overline{\rho_S}}}^{\infty} \frac{1}{\Omega_{c_{SR}}} e^{-\frac{x}{\Omega_{c_{SR}}}}(x)dx \int_{\frac{\psi}{\psi_E \overline{\rho_S} x}}^{\infty} \frac{1}{\Omega_{c_{RD_1}}} e^{-\frac{y}{\Omega_{c_{RD_1}}}}(y)dy \int_0^{\frac{\rho_I}{\overline{\rho_S}}} \frac{1}{\Omega_{c_{SD}}} e^{-\frac{z}{\Omega_{c_{SD}}}}(z)dz$$
$$= -\left(e^{-z\frac{1}{\Omega_{c_{SD}}}} \right)\Bigg|_0^{\frac{\rho_I}{\overline{\rho_S}}} \int_{\frac{\psi}{\overline{\rho_S}}}^{\infty} \frac{1}{\Omega_{c_{SR}}} e^{-\frac{x}{\Omega_{c_{SR}}}}(x)dx \int_{\frac{\psi}{\psi_E \overline{\rho_S} x}}^{\infty} \frac{1}{\Omega_{c_{RD_1}}} e^{-\frac{y}{\Omega_{c_{RD_1}}}}(y)dy$$
$$= \left(1 - e^{-\frac{\rho_I}{\overline{\rho_B}\Omega_{c_{SD}}}} \right) \int_{\frac{\psi}{\overline{\rho_S}}}^{\infty} \frac{1}{\Omega_{c_{SR}}} e^{-\frac{x}{\Omega_{c_{SR}}}} \times \left[-\left(e^{-\frac{y}{\Omega_{c_{RD_1}}}} \right)\Bigg|_{\frac{\psi}{\psi_E \overline{\rho_S} x}}^{\infty} \right](x)dx$$
$$= \left(1 - e^{-\frac{\rho_I}{\overline{\rho_S}\Omega_{c_{SD}}}} \right) \underbrace{\int_{\frac{\psi}{\overline{\rho_S}}}^{\infty} \frac{1}{\Omega_{c_{SR}}} e^{-\frac{x}{\Omega_{c_{SR}}}} e^{-\frac{\psi}{\psi_E \overline{\rho_S} \Omega_{c_{RD_1}} x}}(x)dx}_{A_{11}} \tag{22}$$

Using the series of the exponential and letting t = 1/x,

$$A_{11}=\sum_{n=0}^{\infty}\frac{(-1)^n}{\left(\Omega_{c_{SR}}\right)^{n+1}n!}\int_{\frac{\psi}{\overline{\rho_S}}}^{\infty}x^n e^{-\frac{\mu_1}{x}}dx=\sum_{n=0}^{\infty}\frac{(-1)^n}{\left(\Omega_{c_{SR}}\right)^{n+1}n!}\int_0^{\frac{\psi}{\overline{\rho_S}}}t^{-n-2}e^{-\mu_1 t}dt$$
$$=\sum_{n=0}^{\infty}\frac{(-1)^n}{\left(\Omega_{c_{SR}}\right)^{n+1}n!}\mu_1^{n+1}\gamma\left(-n-1,\frac{\mu_1\psi}{\overline{\rho_S}}\right), \tag{23}$$

which is well-defined via analytic continuation of $\gamma(.,.)$.

Similarly, let

$$A_2=P_r\left(\left|c_{SD}\right|^2>\frac{\rho_I}{\overline{\rho_S}},\left|c_{SR}\right|^2>\frac{\psi\left|c_{SD}\right|^2}{\rho_I},\left|c_{RD_1}\right|^2>\frac{\psi}{\overline{\rho_S}\psi_E\left|c_{SR}\right|^2}\right)$$
$$=\int_{\frac{\rho_I}{\overline{\rho_S}}}^{\infty}f_{|c_{SD}|^2}(x)dx\int_{\frac{\psi x}{\rho_I}}^{\infty}f_{|c_{SR}|^2}(y)dy\int_{\frac{\psi}{\overline{\rho_S}\psi_E y}}^{\infty}f_{|c_{RD_1}|^2}(z)dz$$
$$=\int_{\frac{\rho_I}{\overline{\rho_S}}}^{\infty}\frac{1}{\Omega_{c_{SD}}}e^{-\frac{x}{\Omega_{c_{SD}}}}dx\int_{\frac{\psi x}{\rho_I}}^{\infty}\frac{1}{\Omega_{c_{SR}}}e^{-\frac{y}{\Omega_{c_{SR}}}}dy\int_{\frac{\psi}{\overline{\rho_S}\psi_E y}}^{\infty}\frac{1}{\Omega_{c_{RD_1}}}e^{-\frac{z}{\Omega_{c_{RD_1}}}}dz$$
$$=\int_{\frac{\rho_I}{\overline{\rho_S}}}^{\infty}\frac{1}{\Omega_{c_{SD}}}e^{-\frac{x}{\Omega_{c_{SD}}}}dx\underbrace{\int_{\frac{\psi x}{\rho_I}}^{\infty}\frac{1}{\Omega_{c_{SR}}}e^{-\frac{y}{\Omega_{c_{SR}}}}e^{-\frac{\psi}{\Omega_{c_{RD_1}}\overline{\rho_S}\psi_E y}}dy}_{A21} \tag{24}$$

Proceeding as for A_{11},

$$A_{21}=\sum_{n=0}^{\infty}\frac{(-1)^n}{\left(\Omega_{c_{SR}}\right)^{n+1}n!}\int_{\frac{\psi x}{\rho_I}}^{\infty}x^n e^{-\frac{\mu_1}{x}}dy=\sum_{n=0}^{\infty}\frac{(-1)^n}{\left(\Omega_{c_{SR}}\right)^{n+1}n!}\int_0^{\frac{\rho_I}{\psi x}}t^{-n-2}e^{-\mu_1 t}dt$$
$$=\sum_{n=0}^{\infty}\frac{(-1)^n}{\left(\Omega_{c_{SR}}\right)^{n+1}n!}\mu_1^{n+1}\gamma\left(-n-1,\frac{\mu_1\rho_I}{\psi x}\right) \tag{25}$$

Substituting (25) into (24) yields

$$A_2=\int_{\frac{\rho_I}{\overline{\rho_S}}}^{\infty}\frac{1}{\Omega_{c_{SD}}}e^{-\frac{x}{\Omega_{c_{SD}}}}\left[\sum_{n=0}^{\infty}\frac{(-1)^n}{\left(\Omega_{c_{SR}}\right)^{n+1}n!}\mu_1^{n+1}\gamma\left(-n-1,\frac{\mu_1\rho_I}{\psi x}\right)\right]dx$$
$$=\sum_{n=0}^{\infty}\frac{(-1)^n}{\left(\Omega_{c_{SR}}\right)^{n+1}n!}\mu_1^{n+1}\int_{\frac{\rho_I}{\overline{\rho_S}}}^{\infty}\frac{1}{\Omega_{c_{SD}}}e^{-\frac{x}{\Omega_{c_{SD}}}}\gamma\left(-n-1,\frac{\mu_1\rho_I}{\psi x}\right)dx \tag{26}$$

Therefore, $OP_{D1}=1-(A_1+A_2)$,
which proves Theorem 1. *(Theorem 5 follows by the same steps applied to the corresponding metric; details omitted for brevity.)*

5.2 Appendix B – Proofs of Theorem 2

We have

$$OP_{D_2}=P_r(\min(\gamma_{R,x_2},\gamma_{RD_2,x_2})<\gamma_2=1-\Pr(\gamma_{R,x_2}>\gamma_2,\gamma_{RD2,x_2}>\gamma_2)$$
$$=1-\left[\begin{array}{l}\Pr\left(\overline{\rho_S}\alpha_2\left|c_{SR}\right|^2>\gamma_2,\overline{\rho_S}\alpha_2\left|c_{SR}\right|^2\left|c_{RD_2}\right|^2\psi_E>\gamma_2,\overline{\rho_S}<\frac{\rho_I}{\left|c_{SD}\right|^2}\right)\\+\Pr\left(\frac{\rho_I\alpha_2\left|c_{SR}\right|^2}{\left|c_{SD}\right|^2}>\gamma_2,\overline{\rho_S}\alpha_2\left|c_{SR}\right|^2\left|c_{RD_2}\right|^2\psi_E>\gamma_2,\overline{\rho_S}>\frac{\rho_I}{\left|c_{SD}\right|^2}\right)\end{array}\right]=1-\left(B_1+B_2\right), \tag{27}$$

With

$$B_1 = \Pr\left(|c_{SR}|^2 > \frac{\gamma_2}{\rho_S\alpha_2}, |c_{RD_2}|^2 > \frac{\gamma_2}{\rho_S\alpha_2\psi_E|c_{SR}|^2}, |c_{SD}|^2 < \frac{\rho_I}{\rho_S} \right)$$

$$\begin{aligned} B_1 &= \int_{\frac{\psi_1}{\rho_S}}^{\infty} f_{|c_{SR}|^2}(x)dx \int_{\frac{\psi_1}{\rho_S\psi_E x}}^{\infty} f_{|c_{RD_2}|^2}(y)dy \int_0^{\frac{\rho_I}{\rho_S}} f_{|c_{SD}|^2}(z)dz \\ &= \int_{\frac{\psi_1}{\rho_S}}^{\infty} \left(\frac{1}{\Omega_{c_{SR}}} e^{-x\frac{1}{\Omega_{c_{SR}}}} \right)(x)dx \times \int_{\frac{\psi_1}{\rho_S\psi_E x}}^{\infty} \left(\frac{1}{\Omega_{c_{RD_2}}} e^{-y\frac{1}{\Omega_{c_{RD_2}}}} \right)(y)dy \times \int_0^{\frac{\rho_I}{\rho_S}} \left(\frac{1}{\Omega_{c_{SD}}} e^{-z\frac{1}{\Omega_{c_{SD}}}} \right)(z)dz \\ &= \left(1 - e^{-\frac{\rho_I}{\rho_S\Omega_{c_{SD}}}} \right) \underbrace{\int_{\frac{\psi_1}{\rho_S}}^{\infty} \left(\frac{1}{\Omega_{c_{SR}}} e^{-\frac{x}{\Omega_{c_{SR}}} - \frac{\psi_1}{\Omega_{c_{RD_2}}\rho_S\psi_E x}} \right)}_{B_{11}} \end{aligned} \tag{28}$$

As before,

$$B_{11} = \left(1 - e^{-\frac{\rho_I}{\rho_S\Omega_{c_{SD}}}} \right) \left[\sum_{n=0}^{\infty} \frac{(-1)^n}{\left(\Omega_{c_{SR}}\right)^{n+1} n!} \mu_2^{n+1} \gamma\left(-n-1, \frac{\mu_1\psi_1}{\rho_S} \right) \right]. \tag{29}$$

And

$$\begin{aligned} B_2 &= \Pr\left(|c_{SD}|^2 > \frac{\rho_I}{\rho_S}, |c_{SR}|^2 > \frac{\psi_1|c_{SD}|^2}{\rho_I}, |c_{RD_2}|^2 > \frac{\psi_1}{\rho_S\psi_E|c_{SR}|^2} \right) \\ &= \int_{\frac{\rho_I}{\rho_S}}^{\infty} f_{|c_{SD}|^2}(x)dx \times \int_{\frac{\psi_1 x}{\rho_I}}^{\infty} f_{|c_{SR}|^2}(y)dy \times \int_{\frac{\psi_1}{\rho_S\psi_E y}}^{\infty} f_{|c_{RD_2}|^2}(z)dz \\ &= \int_{\frac{\rho_I}{\rho_S}}^{\infty} \frac{1}{\Omega_{c_{SD}}} e^{-\frac{x}{\Omega_{c_{SD}}}} dx \times \int_{\frac{\psi_1 x}{\rho_I}}^{\infty} \frac{1}{\Omega_{c_{SR}}} e^{-\frac{y}{\Omega_{c_{SR}}} - \frac{\psi_1}{\Omega_{c_{RD_2}}\rho_S\psi_E y}} dy \\ &= \int_{\frac{\rho_I}{\rho_S}}^{\infty} \frac{1}{\Omega_{c_{SD}}} e^{-\frac{x}{\Omega_{c_{SD}}}} \left[\sum_{n=0}^{\infty} \frac{(-1)^n}{\left(\Omega_{c_{SR}}\right)^{n+1} n!} \mu_2^{n+1} \gamma\left(-n-1, \frac{\mu_2\rho_I}{\psi_1 x} \right) \right] dx \\ &= \sum_{n=0}^{\infty} \frac{(-1)^n}{\left(\Omega_{c_{SR}}\right)^{n+1} n!} \mu_2^{n+1} \int_{\frac{\rho_I}{\rho_S}}^{\infty} \frac{1}{\Omega_{c_{SD}}} e^{-\frac{x}{\Omega_{c_{SD}}}} \gamma\left(-n-1, \frac{\mu_2\rho_I}{\psi_1 x} \right) dx \end{aligned} \tag{30}$$

Substituting (28)–(30) into (27) proves Theorem 2.

5.3 Appendix C – Proofs of Theorem 3

We have

$$R_{D_1} = E[\log_2(1+\mathrm{X})], X \triangleq \min(\gamma_{R,x_1}, \gamma_{RD_1,x_1}) = \frac{1}{\ln 2}\int_0^{\infty} \frac{1-F_X(x)}{1+x} dx \tag{31}$$

The CDF $F_X(x)$ is

$$F_X(x) = 1 - [I_{11} + I_{12}], \tag{32}$$

where, letting $\tau = \frac{x}{(\alpha_1 - x\alpha_2)}$ with $\alpha_1 - x\alpha_2 > 0$,

$$\begin{aligned} I_{11} &= U\left(\frac{\alpha_1}{\alpha_2}-x\right)\Pr\left(\left|c_{SR}\right|^2 > \frac{\tau}{\overline{\rho}_S}, \left|c_{RD_1}\right|^2 > \frac{\tau}{\psi_E \overline{\rho}_S \left|c_{SR}\right|^2}, \left|c_{SD}\right|^2 < \frac{\rho_I}{\overline{\rho}_S}\right) \\ &= U\left(\frac{\alpha_1}{\alpha_2}-x\right)\left(\int_{\frac{\tau}{\overline{\rho}_S}}^{\infty} f_{|c_{SR}|^2}(y)dy \times \int_{\frac{\tau}{\psi_E \overline{\rho}_S y}}^{\infty} f_{|c_{RD_1}|^2}(z)dz \times \int_0^{\frac{\rho_I}{\overline{\rho}_S}} f_{|c_{SD}|^2}(u)du\right) \\ &= U\left(\frac{\alpha_1}{\alpha_2}-x\right)\left(1-e^{-\frac{\rho_I}{\overline{\rho}_S \Omega_{c_{SD}}}}\right)\left(\int_{\frac{\tau}{\overline{\rho}_S}}^{\infty} \frac{1}{\Omega_{c_{SR}}} e^{-\frac{y}{\Omega_{c_{SR}}}} e^{-\frac{\tau}{\psi_E \overline{\rho}_S \Omega_{c_{RD_1}} y}}(y)dy\right) \end{aligned} \tag{33}$$

And

$$\begin{aligned} I_{12} &= U\left(\frac{\alpha_1}{\alpha_2}-x\right)\left(\int_{\frac{\rho_I}{\overline{\rho}_S}}^{\infty} f_{|c_{SD}|^2}(y)dy \int_{\frac{\tau y}{\rho_I}}^{\infty} f_{|c_{SR}|^2}(z)dz \int_{\frac{\tau}{\overline{\rho}_S \psi_E z}}^{\infty} f_{|c_{RD_1}|^2}(u)du\right) \\ &= U\left(\frac{\alpha_1}{\alpha_2}-x\right)\left(\int_{\frac{\rho_I}{\overline{\rho}_S}}^{\infty} \frac{1}{\Omega_{c_{SD}}} e^{-\frac{y}{\Omega_{c_{SD}}}} dy \int_{\frac{\tau y}{\rho_I}}^{\infty} \frac{1}{\Omega_{c_{SR}}} e^{-\frac{z}{\Omega_{c_{SR}}}} e^{-\frac{\tau}{\Omega_{c_{RD_1}} \overline{\rho}_S \psi_E z}} dz\right) \end{aligned} \tag{34}$$

Substituting (32)–(34) into (31) yields the closed form in (17), proving Theorem 3.

5.4 Appendix D – Proofs of Theorem 4

We have

$$R_{D_2} = E[\log_2(1+\mathrm{X})], X \triangleq \min\left(\gamma_{R,x_2}, \gamma_{RD_2,x_2}\right) \tag{35}$$

The CDF of X is

$$F_X(x) = 1 - \left[K_{11} + K_{12}\right], \tag{36}$$

where $\tau_1 = \frac{x}{\alpha_2}$,

$$\begin{aligned} K_{11} &= U\left(\frac{\alpha_1}{\alpha_2}-x\right)\Pr\left(\left|c_{SR}\right|^2 > \frac{\tau_1}{\overline{\rho}_S}, \left|c_{RD_1}\right|^2 > \frac{\tau_1}{\psi_E \overline{\rho}_S \left|c_{SR}\right|^2}, \left|c_{SD}\right|^2 < \frac{\rho_I}{\overline{\rho}_S}\right) \\ &= U\left(\frac{\alpha_1}{\alpha_2}-x\right)\left(\int_{\frac{\tau_1}{\overline{\rho}_S}}^{\infty} f_{|c_{SR}|^2}(y)dy \times \int_{\frac{\tau_1}{\psi_E \overline{\rho}_S y}}^{\infty} f_{|c_{RD_1}|^2}(z)dz \times \int_0^{\frac{\rho_I}{\overline{\rho}_S}} f_{|c_{SD}|^2}(u)du\right) \\ &= U\left(\frac{\alpha_1}{\alpha_2}-x\right)\left(1-e^{-\frac{\rho_I}{\overline{\rho}_B \Omega_{c_{SD}}}}\right)\left(\int_{\frac{\tau_1}{\overline{\rho}_B}}^{\infty} \frac{1}{\Omega_{c_{SR}}} e^{-\frac{y}{\Omega_{c_{SR}}}} e^{-\frac{\tau_1}{\psi_E \overline{\rho}_B \Omega_{c_{RD_1}} y}}(y)dy\right) \end{aligned} \tag{37}$$

And

$$\begin{aligned} K_{12} &= U\left(\frac{\alpha_1}{\alpha_2}-x\right)\left(\int_{\frac{\rho_I}{\rho_S}}^{\infty} f_{|c_{SD}|^2}(y)dy \int_{\frac{\tau_1 y}{\rho_I}}^{\infty} f_{|c_{SR}|^2}(z)dz \int_{\frac{\tau_1}{\rho_S \psi_E z}}^{\infty} f_{|c_{RD_1}|^2}(u)du\right) \\ &= U\left(\frac{\alpha_1}{\alpha_2}-x\right)\left(\int_{\frac{\rho_I}{\rho_S}}^{\infty} \frac{1}{\Omega_{c_{SD}}} e^{-\frac{y}{\Omega_{c_{SD}}}} dy \int_{\frac{\tau_1 y}{\rho_I}}^{\infty} \frac{1}{\Omega_{c_{SR}}} e^{-\frac{z}{\Omega_{c_{SR}}}} e^{-\frac{\tau_1}{\Omega_{c_{RD_1}} \rho_S \psi_E z}} dz\right) \end{aligned} \tag{38}$$

Substituting (36)-(38) into (35) gives (19), completing the proof.

References

[1] J. Li, H. H. Chen and Q. Guo, "On the Performance of NOMA Systems with Different User Grouping Strategies," IEEE Wireless Communications, vol. 31, no. 1, pp. 56–61, 2024, doi:10.1109/MWC.010.2200185.

[2] H. Q. Tran, T.-T. Nguyen, C. V. Phan and Q.-T. Vien, "Power-splitting relaying protocol for wireless energy harvesting and information processing in NOMA systems," IET Communications, vol. 13, no. 14, pp. 2132–2140, 2019.

[3] H. Q. Tran, C. V. Phan, and Q.-T. Vien, "Power splitting versus time switching based cooperative relaying protocols for SWIPT in NOMA systems," Physical Communication, 2020, doi:10.1016/j.phycom.2020.101098.

[4] Z. Gao, H. Wang, Y. Chen, L. Fan and R. Zhao, "Maximizing Long-Term Average System Communication Capacity of SWIPT-Enabled AF Relay System via Lyapunov Optimization," IEEE Internet of Things Journal, vol. 11, no. 3, pp. 4679–4692, 2024.

[5] H. Q. Tran, "PSR versus TSR Relaying Protocols: Leveraging Full-Duplex DF and Energy Harvesting for SWIPT in NOMA Systems," Wireless Personal Communications, vol. 134, pp. 293–318, 2024.

[6] H. Q. Tran, S. N. Sur, and B. M. Lee, "A Comprehensive Analytical Framework under Practical Constraints for a Cooperative NOMA System Empowered by SWIPT IoT," Mathematics, vol. 12, art. 2249, 2024.

[7] S. N. Sur, H. Q. Tran, A. L. Imoize, D. Kandar, and S. Nandi, "Sum-Rate Maximization for a Hybrid Precoding-Based Massive MIMO NOMA System with Simultaneous Wireless Information and Power Transmission," Telecom, vol. 5, pp. 823–845, 2024.

[8] F. Qi, L. Liu, W. Xie and Z. Sun, "Fountain Coded Coordinated Multipoint for 5G MBMS UAV Relay," IEEE Transactions on Broadcasting, vol. 70, no. 1, pp. 99–109, 2024.

[9] A. Andrawes, R. Nordin, and N. F. Abdullah, "Energy-Efficient Downlink for Non-Orthogonal Multiple Access with SWIPT under Constrained Throughput," Energies, vol. 13, no. 1, art. 107, 2020.

[10] Z. Albataineh, A. Andrawes, N. F. Abdullah, and R. Nordin, "Energy-Efficient Beyond 5G Multiple Access Technique with Simultaneous Wireless Information and Power Transfer for the Factory of the Future," Energies, vol. 15, art. 6059, 2022.

[11] A. Andrawes, R. Nordin, and M. Ismail, "Wireless Energy Harvesting with Cooperative Relaying under the Best Relay Selection Scheme," Energies, vol. 12, no. 5, art. 892, 2019.

[12] X. Pei, W. Duan, M. Wen, Y.-C. Wu, H. Yu, and V. Monteiro, "Socially Aware Joint Resource Allocation and Computation Offloading in NOMA-Aided Energy-Harvesting Massive IoT," IEEE Internet of Things Journal, vol. 8, no. 7, pp. 5240–5249, 2021.

[13] F. Tan, P. Wu, Y.-C. Wu and M. Xia, "Energy-Efficient Non-Orthogonal Multicast and Unicast Transmission of Cell-Free Massive MIMO Systems with SWIPT," IEEE Journal on Selected Areas in Communications, vol. 39, no. 4, pp. 949–968, 2021.

[14] Z. Ding, X. Lei, G. K. Karagiannidis, R. Schober, J. Yuan and V. K. Bhargava, "A Survey on Non-Orthogonal Multiple Access for 5G Networks: Research Challenges and Future Trends," IEEE Journal on Selected Areas in Communications, vol. 35, no. 10, pp. 2181–2195, 2017.

[15] P. Xu, Y. Yuan, Z. Ding, X. Dai and R. Schober, "On the Outage Performance of Non-Orthogonal Multiple Access With 1-bit Feedback," IEEE Transactions on Wireless Communications, vol. 15, no. 10, pp. 6716–6730, 2016.

[16] M. Basharat et al., "Non-Orthogonal Radio Resource Management for RF Energy Harvested 5G Networks," IEEE Access, vol. 7, pp. 46550–46561, 2019.

[17] P. Devasis and K. C. Priyanka, "RF-Energy Harvesting (RF-EH) for Sustainable Ultra Dense Green Network (SUDGN) in 5G Green Communication," Saudi Journal of Engineering and Technology, vol. 5, no. 6, 2020.

[18] D. Li, "Performance Analysis of MRC Diversity for Cognitive Radio Systems," IEEE Transactions on Vehicular Technology, vol. 61, no. 2, pp. 849–853, 2012.

[19] D. Li, "Opportunistic DF–AF Selection for Cognitive Relay Networks," IEEE Transactions on Vehicular Technology, vol. 65, no. 4, pp. 2790–2796, 2016.

[20] D. Li, "Amplify-and-Forward Relay Sharing for Both Primary and Cognitive Users," IEEE Transactions on Vehicular Technology, vol. 65, no. 4, pp. 2796–2801, 2016.

[21] S. Vahidian, E. Soleimani-Nasab, S. Aïssa and M. Ahmadian-Attari, "Bidirectional AF Relaying with Underlay Spectrum Sharing in Cognitive Radio Networks," IEEE Transactions on Vehicular Technology, vol. 66, no. 3, pp. 2367–2381, 2017.

[22] A. Pandey, S. Yadav, D.-T. Do and R. Kharel, "Secrecy Performance of Cooperative Cognitive AF Relaying Networks With Direct Links Over Mixed Rayleigh and Double-Rayleigh Fading Channels," IEEE Transactions on Vehicular Technology, vol. 69, no. 12, pp. 15095–15112, 2020.

[23] A. Prathima, D. S. Gurjar, H. H. Nguyen and A. Bhardwaj, "Performance Analysis and Optimization of Bidirectional Overlay Cognitive Radio Networks With Hybrid-SWIPT," IEEE Transactions on Vehicular Technology, vol. 69, no. 11, pp. 13467–13481, 2020.

[24] V. S. Nguyen and T. H. Nguyen, "Performance Analysis of Cognitive-Inspired Wireless Powered NOMA Systems with Joint Collaboration," IEEE Access, vol. 11, pp. 51578–51589, 2023.

[25] L. Dai, B. Gui and L. J. Cimini, Jr., "Selective Relaying in OFDM Multihop Cooperative Networks," in Proc. IEEE WCNC, 2007, pp. 963–968.

[26] S. Gautam, E. Lagunas, S. Chatzinotas and B. Ottersten, “Relay Selection and Resource Allocation for SWIPT in Multi-User OFDMA Systems,” IEEE Transactions on Wireless Communications, vol. 18, no. 5, pp. 2493–2508, 2019.
[27] Y. Su, L. Jiang and C. He, “Decode-and-Forward Relaying with Full-Duplex Wireless Information and Power Transfer,” IET Communications, vol. 11, no. 13, pp. 2110–2115, 2017.
[28] S. Kusaladharma and C. Tellambura, “Energy Harvesting Aided by Random Motion: A Stochastic Geometry Based Approach,” IEEE Transactions on Green Communications and Networking, 2020.
[29] T. D. P. Perera, D. N. K. Jayakody, S. K. Sharma, S. Chatzinotas and J. Li, “SWIPT: Recent Advances and Future Challenges,” IEEE Communications Surveys & Tutorials, vol. 20, no. 1, pp. 264–302, 2018.
[30] A. A. Nasir, X. Zhou, S. Durrani and R. A. Kennedy, “Relaying Protocols for Wireless Energy Harvesting and Information Processing,” IEEE Transactions on Wireless Communications, vol. 12, no. 7, pp. 3622–3636, 2013.
[31] C. Guo, L. Zhao, C. Feng, Z. Ding and H.-H. Chen, “Energy Harvesting Enabled NOMA Systems With Full-Duplex Relaying,” IEEE Transactions on Vehicular Technology, vol. 68, no. 7, pp. 7179–7183, 2019.
[32] B. Clerckx, R. Zhang, R. Schober, D. W. K. Ng, D. I. Kim and H. V. Poor, “Fundamentals of Wireless Information and Power Transfer: From RF Energy Harvester Models to Signal and System Designs,” IEEE Journal on Selected Areas in Communications, vol. 37, no. 1, pp. 4–33, 2019.
[33] J. M. Kang, I. M. Kim and D. I. Kim, “Joint Tx Power Allocation and Rx Power Splitting for SWIPT System with Multiple Nonlinear Energy Harvesting Circuits,” IEEE Wireless Communications Letters, vol. 8, no. 1, pp. 53–56, 2019.
[34] G. Ma, J. Xu, Y. Zeng and M. R. V. Moghadam, “A Generic Receiver Architecture for MIMO Wireless Power Transfer with Nonlinear Energy Harvesting,” IEEE Signal Processing Letters, vol. 26, no. 2, pp. 312–316, 2019.
[35] F. Fang, H. Zhang, J. Cheng, S. Roy and V. C. M. Leung, “Joint User Scheduling and Power Allocation Optimization for Energy-Efficient NOMA Systems With Imperfect CSI,” IEEE Journal on Selected Areas in Communications, vol. 35, no. 12, pp. 2874–2885, 2017.
[36] I. S. Gradshteyn and I. M. Ryzhik, Table of Integrals, Series and Products, 6th ed., Academic Press, San Diego, 2000.

Authors’ Profiles

Huu Q. Tran (Member, IEEE) received the M.S. degree in Electronics Engineering from Ho Chi Minh City University of Technology and Education (HCMUTE), Vietnam in 2010. Currently, he has been working as a lecturer at Faculty of Electronics Technology, Industrial University of Ho Chi Minh City (IUH), Vietnam. He obtained his doctorate from the Faculty of Electrical and Electronics Engineering at HCMUTE, Vietnam. His research interests include wireless communications, non-orthogonal multiple access (NOMA), energy harvesting (EH), wireless cooperative relaying networks, heterogeneous networks (HetNet), cloud radio access networks (C-RAN), unmanned aerial vehicles (UAV), reconfigurable intelligent surfaces (RIS), short-packet communication (SPC) and internet of things (IoT).

Lam Hoang Kham received the B.S. degree in Electronic and Telecommunication Engineering Technology from the Industrial University of Ho Chi Minh City (IUH), Vietnam, in 2014. He is currently pursuing his master's degree at IUH and working as a researcher at Furitek, Vietnam. His research interests include wireless communications, non-orthogonal multiple access (NOMA), energy harvesting (EH), wireless cooperative relaying networks, hardware design, embedded programming, and the Internet of Things (IoT).

How to cite this paper: Huu Q. Tran, Lam Hoang Kham, "Empowering Next-Gen Networks: Unleashing the Potential of SWIPT-Enabled Energy Harvesting in Collaborative Cognitive Radio-NOMA Networks", International Journal of Wireless and Microwave Technologies(IJWMT), Vol.15, No.6, pp. 27-40, 2025. DOI:10.5815/ijwmt.2025.06.03